This manuscript was accepted by J. Appl. Phys. Click here to see the version of record.

Structural and electrical characterization of polycrystalline NbO_2 thin film vertical devices grown on TiN-coated SiO_2/Si substrates

Toyanath Joshi[1], Pavel Borisov[2], and David Lederman[1]

[1]*Department of Physics, University of California Santa Cruz, Santa Cruz, CA 95064, USA*
[2]*Department of Physics, Loughborough University, Loughborough, LE11 3TU, UK*

We report on the electrical properties of polycrystalline NbO_2 thin film vertical devices grown on TiN coated SiO_2/Si substrates using pulsed laser deposition. First, we analyzed the thickness and contact size dependences of threshold switching of NbO_2 films grown in 10 mTorr Ar/O_2 mixed growth pressure, where 25.1%/74.9% of NbO_2/Nb_2O_5 surface composition content was estimated by *ex-situ* x-ray photoelectron spectroscopy. The threshold switching and self-sustained current oscillatory behavior of films with different NbO_2/Nb_2O_5 composition ratios was measured and analyzed. The current-voltage measurement revealed that the leakage current property in the insulating state was dominated by trap-charge assisted Poole-Frankel (P-F) conduction mechanism. All films showed threshold switching behavior in agreement with the previously proposed joule heating mechanism. The second film was grown in lower (1 mTorr) growth pressure which resulted in a higher (34.2%/65.8%) NbO_2/Nb_2O_5 film surface composition. The film grown in higher growth pressure demonstrated lower off-state leakage current, faster switching, and self-sustained oscillations with higher frequency than the film grown in lower growth pressure.

This manuscript was accepted by J. Appl. Phys. Click here to see the version of record.

I. Introduction

Transition metal oxides demonstrating metal-to-insulator transitions (MIT), such as VO_2[1-3] and NbO_2, are widely studied materials for the use as selector elements in resistive random-access memory (RRAM) and in current oscillatory devices.[1-14] VO_2 has shown changes on the order of 10^5 in resistivity around T_{MIT} = 340 K.[1] The MIT temperature of VO_2, however, is close to room temperature and can be easily reached by heat dissipation while used in electronic devices. NbO_2, on the other hand, has a much higher MIT temperature (T_{MIT} = 1081 K)[15,16] making this material a robust candidate for current threshold switching devices.[4-20]

Previously reported NbO_2 thin film vertical devices have been composed of amorphous NbO_2 films.[4-7,10-14] Detailed investigations on polycrystalline thin film devices, however, is still lacking. Here, we report on the structural and electrical properties of NbO_2 polycrystalline thin films grown using PLD on TiN coated SiO_2/Si substrates, a platform important for the further development of electronic devices based on NbO_2. This study is focused on the threshold switching and leakage current characteristics of NbO_2 vertical devices, mainly after the forming process. We pursued three promising routes for optimizing the device performance by (1) varying thickness of the film, (2) varying the size of top electrode metallic contacts, and (3) varying Nb^{4+}/Nb^{5+} content ratio.

II. Experimental details

TiN (11 nm)/SiO_2(100nm)/Si wafers, provided by Micron Technology, were used as substrates for NbO_2 thin film growth using pulsed laser deposition. A ceramic target of

This manuscript was accepted by J. Appl. Phys. Click here to see the version of record.

Nb_2O_5 was prepared from Nb_2O_5 powder (99.99%, Sigma-Aldrich). The powder was pressed into a pellet and sintered for 72 h in air at 1300 °C. The distance between the target and the substrate was 7.3 cm. The KrF laser energy density at the target was approximately 2 J/cm^2 and its pulse repetition rate was 5 Hz. The substrate temperature was kept at 700 °C. A set of films with different thicknesses was grown in 10 mTorr O_2/Ar mixed gas atmosphere with 7% O_2 mass flow. A 1 mTorr growth pressure with 7% O_2 mass flow was used in order to examine the effects of possible oxygen vacancies.

A four-axis goniometer x-ray diffraction (XRD) system with a Cu K_α rotating anode was used for structural characterization of the deposited films. Out-of-plane (θ-2θ) and grazing incidence x-ray diffraction (GIXRD) scans were performed. Polycrystalline peaks of NbO_2 were verified from the powder diffraction file PDF# 00-043-1043.[21] Film thickness and surface roughness analysis were performed on x-ray reflectivity (XRR) data obtained from the same x-ray diffraction system.

The chemical composition of the films was analyzed using x-ray photoelectron spectroscopy (XPS) measured in a PHI 5000 VersaProbe spectrometer from Physical Electronics. The spectra were calibrated using C 1s peak at 284.8 eV and fitted under the assumption of a Shirley-type background. Areas under each curve were compared to obtain molar ratios between different Nb oxides present in the films.

The current-voltage (*I*-*V*) characteristics and current oscillations were measured using probe station tungsten tips (Picoprobe) from GGB Industries Inc. which were pressed directly on top of the film. The nominal lateral size of the probe station tip used was ~2 µm. The voltage was applied across the thin film at ramp rates of 0.1 V/sec and

This manuscript was accepted by J. Appl. Phys. Click here to see the version of record.

the output current was measured across an attached serial test resistance of R_s = 51 Ω. For pulsed *I-V* measurements, short triangular ramp pulses were applied to the sample and the output current was measured using a digital oscilloscope.

Contact-size dependent *I-V* measurements were performed with a voltage loop frequency of 1 Hz using an atomic force microscopy instrument from Asylum equipped with conducting platinum coated Si cantilever tips. Top circular Pt electrodes were sputtered to 50 nm thickness with diameters ranging from 6.5 µm to 0.1 µm using electron-beam lithography.

III. Results and discussion

A. Structural and chemical analysis

Figure 1 shows θ-2θ and grazing incidence x-ray diffraction (GIXRD) scans of two of the NbO_2 films grown on $TiN/SiO_2/Si$ substrates in 1 and 10 mTorr $Ar+O_2$ (~7% O_2) pressures and having thicknesses 43.7 and 33.2 nm, respectively. Both films showed preferential growth along (100) and (110) crystallographic planes. Consequently, the expected (222)-peak at 35.2° was not present or perhaps had a very low intensity both in the out-of-plane and grazing incidence scans. No peaks related to Nb_2O_5 or NbO phases were observed. The presence of SiO_2 peaks in the 10 mTorr sample are explained by SiO_2 crystallization at the growth substrate temperature in an oxygen atmosphere. Note the absence of SiO_2 peaks in the film grown in 1 mTorr pressure due to the lower O_2 growth pressure.

Figure 2 shows x-ray reflectivity curves for the samples with the thickness ranging from 13.7 to 76.4 nm grown into 10 mTorr and a 43.7 nm film grown in 1 mTorr (blue

open circles symbol). Fitting (solid curves) to an optical model was performed using GenX software.[22] The bottom TiN layer had a thickness of 11 nm with an interface roughness at the TiN/NbO_2 interface of ~0.4 nm. The maximum surface roughness was approximately 1 nm for the 76.4 nm thick film. The best fit was achieved assuming an additional top layer with approximately 2.7 nm thick which is most likely a Nb_2O_5 layer formed by oxidation of NbO_2 after exposure to the atmosphere. The inset in Fig. 2 shows a cross-sectional SEM image of 76.4 nm film. All four layers Si, SiO_2, TiN, and NbO_2 are visible with the corresponding thicknesses agreeing with the nominal values. It is difficult to unequivocally ascertain whether the top Nb_2O_5 layer is visible in the SEM image.

The molar content of NbO_2 and Nb_2O_5 phases was obtained using XPS spectra taken at the 3d core Nb level. XPS spectra measured on the films grown in 1 and 10 mTorr total growth pressures are shown in Fig. 3(a) and 3(b), respectively. The deconvoluted peak fits for the film grown in 10 mTorr pressure show $3d_{3/2}$ and $3d_{5/2}$ peaks from the Nb^{4+} state at 205.6 and 208.3 eV, respectively, in agreement with previous reports.[19,23] Large peaks at 207.1 and 209.8 eV were observed corresponding to Nb^{5+}, probably due to the oxidation of the film surface to Nb_2O_5 after exposure to the atmosphere. The shaded areas mark the peaks related to Nb^{4+} which correspond to the NbO_2 phase. The approximate content of NbO_2 and Nb_2O_5 was calculated using the area covered by $3d_{5/2}$ level peaks and yielded the values of 34.2%/65.8% and 25.1%/74.9% for the films grown in 1 and 10 mTorr growth pressures, respectively. Peaks related to Nb_2O_5 were not visible in XRD or GIXRD spectra in Fig. 1. This suggests that either the Nb_2O_5 top layer was amorphous or at least polycrystalline. Other authors have reported the estimated

This manuscript was accepted by J. Appl. Phys. Click here to see the version of record.

thickness of the top Nb_2O_5 layer to be ≈2 nm.[24] The exact estimation of the oxygen stoichiometry, however, is difficult via *ex-situ* measurements due to the possibility of the film surface oxidation after exposure to the air.

B. Film thickness effect on current threshold switching

First, we analyzed *I-V* characteristics measured on NbO_2 films [Fig. 4(a)] with film thicknesses of 13.7, 33.2 and 76.4 nm grown in 10 mTorr total Ar+O_2 pressure. The measurements were taken using the probe station tungsten tip placed directly on the surface of the samples as a top electrode and TiN layer as a bottom contact. Pt contacts were not used for these measurements. Clear threshold switching in the output current was observed and the threshold switching voltage (V_{th}) depended linearly on the film thickness [Fig. 4(b)]. The linear dependence of V_{th} indicated the bulk portion of the film took part in the switching, rather than the metal-oxide interface. This contrasts with some other materials, for example Fe_2O_3,[25] which have a resistive switching behavior that is independent of the film thickness because the metal-oxide interface dominates the switching. The current measured at constant voltage [0.9 V in Fig. 4(b)], on the other hand, showed an exponential decrease with the square root of the film thickness which meant $I \sim \exp(\beta E^{\frac{1}{2}})$, where β is a constant. This indicated that the current carriers were electrons following Poole-Frankel (P-F) conduction rather than ions. The mobility of the ionic current carriers, in contrast, varies as $\exp(\beta E)$ as reported in Ref. 26.

Prior to observing a threshold switching, a forming pulse was needed,[20] requiring the application of larger electric field magnitudes than those used during normal operation [dotted curves in Fig. 4(a)]. It is believed that during the electroforming step,

This manuscript was accepted by J. Appl. Phys. Click here to see the version of record.

an accumulation of defects, such as oxygen vacancies, takes place which creates a conductive current path, called filaments. Also, dielectric breakdown of the top Nb_2O_5 layer might take place during forming.[27] The forming voltage dependence on thickness, however, indicated that the top surface was not the only mechanism responsible for the forming step. In fact, a forming step was also observed in lateral devices where the top layer played no role at all because current flowed in-plane direction. [28]

Low voltage ($V < V_{th}$) regions of *I-V* curves of the samples with different thicknesses were fitted to ohmic ($I \sim V$), space-charge-limited ($I \sim V^2$), Schottky [$I \sim \exp(\beta V^{\frac{1}{2}})$], and Poole-Frankel conduction [$I \sim V\exp(\beta V^{1/2})$] models. Fig. 4(c) shows a $\ln(I)$ vs. $V^{1/2}$ curve (symbols with open circles) and the fit for the 33.2 nm film. For all three thicknesses, the P-F model[29,30] resulted in the best fit which suggested that the high resistance state conduction was due to field-assisted hoping of carriers from Coulomb trap centers.[10] Several other authors also have claimed that P-F is the dominant conduction mechanism in crystalline[10] as well as in amorphous films[31-33] of NbO_x.

Our previous study of NbO_2 lateral devices[19,20] demonstrated that the threshold switching was triggered by Joule heating produced by current flowing through the devices. In the low bias voltage region, the P-F model fit the data well as discussed above. A slight increased nonlinearity in current characteristics [above 1 V, Fig. 1(c)] was probably due to the added contribution of the increased temperature by Joule heating.

C. Top contact size effect on current threshold switching

To construct the clear image of filamentary nature in NbO_2 devices, the threshold switching dependence on contact size was investigated using the conducting probe AFM

This manuscript was accepted by J. Appl. Phys. Click here to see the version of record.

technique. For these measurements, the current compliance was set to 10 μA, the maximum allowed by the AFM instrument. *I-V* curves obtained from the 10 mTorr growth pressure sample using top contact diameters d ranging from 0.1 μm to 6.5 μm are shown in Fig. 5(a). Abrupt switching was not visible, especially for the larger contacts, because of the lower compliance of the current limit. These data, however, were acquired after completion of the forming step [see Fig. 6(b)] and therefore resembled threshold switching of NbO_2 film. Further measurements with higher current compliance are required to confirm the area dependence of the threshold switching.

Leakage currents measured at $V = 0.3$ V as a function of contact area A are shown in the Fig. 5(b). The data fitted well on a log-log scale to two power-law segments of the form $\ln(I) = n\ln(A) + C$, where n is the exponent in the power-law, A is the contact area, and C is a constant. For larger area contacts with $A > 2.8 \times 10^{-9}$ cm^2, exponent $n_1 = 0.82 \pm 0.06$, or $I \sim d^2$, whereas for smaller area contacts with $A \leq 2.8 \times 10^{-9}$ cm^2, $n_2 = 0.51 \pm 0.02$, or $I \sim d$. Thus, below the critical area of $A = 2.8 \times 10^{-9}$ cm^2 [$d = 0.6$ μm, the dotted line in Fig. 5(b)], the current was proportional to the diameter rather than the area of the contact. Similar studies on $NbO_2/TiO_x/NbO_2$[34] trilayers had revealed that the current depended on the electrode area ($I \propto A$), which implied that the number of carrier traps per unit area, which were responsible for the oxide conductivity, was approximately constant. Thus, the parallel current filamentary pathways were created homogeneously across the area of the contact which could be explained in term of the 'Closed Faucet' type model as discussed by Inoue et al. in Ref. 25. On the other hand, if $I \propto A^n$ with $n < 1$ (e.g., $n = 0.3$ in Ref. 34 for a low resistance

This manuscript was accepted by J. Appl. Phys. Click here to see the version of record.

state), the current was not uniform across the contact area. In our case, $n \approx 0.5$, which may indicate that electrode edges were the regions which dominate low-field conduction, in which case the current was proportional to the contact's circumference and therefore $I \propto d \propto A^{1/2}$. A transformation to $n \approx 1$ for diameters $d > 0.6$ μm then corresponds to the diminished influence of the contact edge in larger electrodes. Other reports[12,34] consisted of modifying the bottom electrodes, and so they could have encountered an additional effect due to different film growth mode in the resistive switching layer.

In any case, the dependence of current on contact size is of technological importance. In Si-based FinFET devices, for example, reduction in device dimension results in increased leakage current due to the quantum tunneling of the electrons between the gates. In the case of the NbO_2 device, however, lowering the lateral device dimension not only increases the device density but also lowers the leakage current. Using the smallest contact size (i.e., AFM tip), the leakage current measured at $V_{th} \approx 1.6$ V was $I_{th} \sim 10^{-6}$ A which is an order of magnitude lower than reported elsewhere to date.[5,11-13]

D. Effects of Nb^{5+}/Nb^{4+} content

We also investigated the effect of O_2/Ar total pressure on the *I-V* characteristics. *I-V* characteristics measured on two films grown in 1 and 10 mTorr growth pressure [Fig. 6(a)] were compared using the top contact with a diameter of 0.3 μm. For currents measured at the same voltage, for example at 0.2 V, the film grown in lower growth pressure (1 mTorr) had a current that was an order of magnitude higher than the one measured on the film grown in higher growth pressure (10 mTorr). The larger content of

This manuscript was accepted by J. Appl. Phys. Click here to see the version of record.

insulating Nb_2O_5 was likely responsible for lower leakage current in the film grown in a higher oxygen pressure. On the other hand, a larger defect density, such as O-vacancies, might be responsible for increased leakage current for the film grown in a lower growth pressure. Partial overlap of Coulomb potential wells with increased trap density helps lower the barrier height in the P-F model increasing the conductivity. The bulk film region might have a small amount of conducting NbO or metallic Nb which might be the origin of larger leakage current. It is not possible to estimate exact bulk film stoichiometry using ex-situ XPS measurements because of the surface sensitive nature of XPS. NbO or metallic Nb on the surface of the film would probably be easily oxidized to NbO_2 or Nb_2O_5 upon exposure to the atmosphere.

Forming pulses for the film grown in 10 mTorr measured using 0.3 µm and 6.5 µm contacts are shown in Fig. 6(b). These measurements indicated that the forming voltage also depended on the contact size. The larger diameter top contacts required a smaller voltage during the electroforming step, in agreement with Ref. 12.

We also compared the threshold switching behavior of these films. Figure 7(a) shows a circuit diagram for pulsed IV measurements. Triangular voltage pulses with different pulse widths (τ) were applied across the films and the output current was measured across a test resistor R_s. A non-linear current switching characteristic was observed for pulse widths $\tau \leq 10$ µs. Output pulses for both samples for $\tau \leq 10$ µs are plotted in Fig. 7(b) and 7(d). The device from the film grown in 1 mTorr had a smaller turn-on voltage $V_{ON} = 1.5$ V and a smaller current ON/OFF ratio (~ 5) than the one for the device from the film grown in 10 mTorr pressure, $V_{ON} = 2$ V and a ratio ~ 10. This can be

This manuscript was accepted by J. Appl. Phys. Click here to see the version of record.

explained by the more insulating character of the film grown in 10 mTorr. In addition, the device made from the film grown in 10 mTorr had more abrupt ON- and OFF-switching. An enlarged view of an output current pulse measured on the film grown in 10 mTorr growth pressure is shown in Fig. 7(c). The typical OFF-to-ON switching time (τ_{ON}) was found to be 25 ns, which is fast enough for a current selection element in many RRAM device prototypes.[35] This result held true for 4 other samples grown using similar growth conditions. ON/OFF switching times for the film grown in 1 mTorr [Fig. 7(b)] were approximately twice as long as the ON/OFF times measured for the films grown in 10 mTorr pressure. Here, the switching time is considered only for the extremely sharp region [the shaded region in Fig. 7(c)]. Thus, the device from the film with lower NbO_2 content (grown in 10 mTorr pressure) can provide the better performance if used in a current switching element. Interestingly, a current overshoot was observed in case of the film grown in 10 mTorr growth pressure [Fig. 7(c) and (d)], which was not observed for one grown in 1 mTorr [Fig. 7(b)]. The current overshoot is likely caused by the switching time τ_{ON} being shorter than the associated capacitance (C_p) discharge time ($\sim R_{ON}C_p$).[36] The fact that no overshoot seems to happen for films grown in 1 mTorr pressure is further proof of a slower switching behavior.

We also note that films grown in pressures greater than 10 mTorr had a significant amount of the insulating Nb_2O_5 phase and no threshold switching behavior was observed. A gradual appearance of Nb_2O_5 phase for the epitaxial films grown above 10 mTorr was demonstrated using x-ray diffraction in our previous work.[19]

This manuscript was accepted by J. Appl. Phys. Click here to see the version of record.

E. Self-sustained current oscillations

Finally, we discuss self-sustained current oscillations in our vertical devices. Figure 8(a) shows the connection diagram. The sample was connected in series to a load resistor (R_L) of 10 kΩ and a sensing resistor (R_S) of 51 Ω; the latter was used to measure the current. The sample is shown as a switchable resistor connected to a parallel capacitor, representing the intrinsic capacitance of the insulating (OFF) state. A low-frequency input voltage (V_{in}) with a triangular or rectangular wave shape was applied and the output signal (i.e. current, I_{out}) was measured across R_S.

Figure 8(b) shows a current response after a triangular voltage pulse was applied. Current oscillations were observed only within the range of the input voltage $2\ \mathrm{V} < V_{in} < 5\ \mathrm{V}$ [red, dotted line in zoomed view of Fig. 8(b)]. These oscillations are produced as a result of a thermally induced negative differential resistance.[4,37,38] After the film material temperature increases due to the Joule heating, the current keeps on rising even while the input voltage is decreasing. The device current is highly unstable in this region so that by choosing appropriate circuit parameters, such as R_L and V_{in}, self-sustained current oscillations can be induced.[39]

Figure 8(c) shows the output current characteristics of the film grown in 1 mTorr and measured by applying a rectangular pulse with ~ 9 µs pulse width and 4.4 V in amplitude. Before applying V_{in}, the NbO_2 device was in its initial high resistance state, so the associated capacitor was charged when the voltage was applied. The increase in current caused it to switch to the low resistance state, resulting in a discharge of the capacitor. During this step, the largest voltage V_{in} drop occurred across R_L and so the film

This manuscript was accepted by J. Appl. Phys. Click here to see the version of record.

turned itself insulating when the sample voltage was reduced. A rapid repetition of the process provided oscillations in the output current.

Highly stable oscillations were obtained during positive and negative cycles of the input voltage. Oscillations lasted over 48 hours (10^{12} cycles) with 5% fluctuation in frequency and 33% fluctuation in amplitude, which is the most stable oscillator so far reported for NbO_2. This exceptional stability is likely associated with the polycrystallinity of our films, but a direct comparison between polycrystalline and amorphous films is missing.

The peak-to-peak amplitude (I_{pp}) of current oscillations was about 1.1 mA. A Fast Fourier Transform (FFT) of the signal showed that the fundamental frequency was at 11 MHz [Fig. 8(c)] for an input voltage of 4.5 V. The presence of higher order harmonics is predicted by parallel filamentary model. These harmonics originate from a stochastic resonance produced by internal noise-induced perturbation added to the system.[40] In terms of the parallel filamentary model, each filament acts as an individual but intrinsically coupled (most probably via thermal coupling) oscillator.

We studied the dependence of the oscillation frequency on input voltage in films grown at 1 and 10 mTorr total growth pressures, i.e. in films with different NbO_2-content (Fig. 9). A closer view of oscillations is shown in the inset to Fig. 9 with similar frequencies of ~11 MHz for both films. Aside from the main frequency oscillations, other harmonics were present.

For the film grown in 1 mTorr, the range of V_{in} where oscillations were observed was found to be between 2.5 V to 4.8 V, in agreement with the study on the same film

This manuscript was accepted by J. Appl. Phys. Click here to see the version of record.

under triangular pulse application [Fig. 8(b)]. The oscillation frequency f_{osc} increased with increasing input voltage amplitude V_{in} until $V_{in} = 4$ V. So, for this film, the frequency could be tuned from 6.7 MHz to 13.6 MHz. Upon further increase of V_{in}, f_{osc} started to decrease and oscillations disappeared. A similar trend in frequency variation: linear increment followed by a saturated region has been reported in polycrystalline thin film devices.[41] For the film grown in 10 mTorr, the frequency increased linearly with increasing V_{in} and no saturation region existed. The range of V_{in} resulting in stable oscillations for the film was higher, between 4 V and 7.5 V and the frequency could be tuned from 10 MHz to 18 MHz. Because of the higher Nb_2O_5 content, the film grown in 10 mTorr had a higher threshold voltage and thus a larger range of V_{in} which produced oscillations. Thus, the range of V_{in} over which oscillations were produced was enlarged by using films with different contents of NbO_2.

IV. Conclusions

In conclusion, we have studied structural and electric properties of NbO_2 films grown on TiN coated SiO_2/Si substrate using different growth pressures. $\theta - 2\theta$ and grazing incidence x-ray diffractometry verified the polycrystalline growth of NbO_2. The threshold switching voltage depended on the thickness of the sample and the off-state leakage current was described by the Poole-Frenkel conduction mechanism. The threshold switching behavior of the device depended on the contact size, with a dependence on the diameter of the contact for small contacts and on the area for large contacts. The off-state leakage current could be reduced by increasing film thickness

and/or decreasing the lateral size of the device. Pulsed *I-V* measurements performed on these samples showed a current switching time of ~25 ns. Highly stable self-oscillatory current behavior was demonstrated where the oscillation frequency was tuned in the range of 6.7 to 13.6 MHz for the film grown in 1 mTorr and 10 to 18 MHz for the film grown in 10 mTorr pressure. The presence of higher harmonics can be explained by parallel conducting filaments thermally coupled to each other.

Acknowledgments

This work was supported in part by FAME, one of six centers of STARnet, a Semiconductor Research Corporation program sponsored by MARCO and DARPA (Contract # 2013-MA-2382) and the West Virginia University Shared Research Facilities.

References:

[1]Morin, F. J. Phys. Rev. Lett. 3, 34 (1959)

[2]M. Son, J. Lee, J. Park, J. Shin, G. Choi, S. Jung, W. Lee, S. Kim, S. Park, and H. Hwang, IEEE Electron Device Letters **32**, 1579 (2011)

[3]A. Beaumont, J. Leroy, J.-C. Orlianges, and A. Crunteanu, J. Appl. Phys. **115**, 154502 (2014)

[4]M. D. Pickett, G. Medeiros-Ribeiro and R. S. Williams, *Nat. Mater.* **12**, 114 (2013)

[5]S. Li, X. Liu, S. K. Nandi, D. K. Venkatachalam and R. G. Elliman, Nanotechnology 28, 125201 (2017)

[6]S. Kim, J. Park, J. Woo, C. Cho, W. Lee, J. Shin, G. Choi, S. Park, D. Lee, B. H. Lee, H. Hwang, *Microel. Eng.* **107,** 33 (2013)

[7]X. Liu, S. K. Nandi, D. K. Venkatachalam, K. Belay, S. Song, and R. G. Elliman, IEEE Electron Device Letters 35, 1055 (2014)

[8]H. R. Phillipp, and L. M. Levinson, *J. Appl. Phys.* **50** 4814 (1979)

[9]J. C. Lee, W. W, Durand, *J. Appl. Phys* **56** 3350 (1984)

[10]S. H. Shin, T. Halpern, and P. M. Raccah, *J. Appl. Phys.* 48, 3150 (1977)

[11]X. Liu, S. M. Sadaf, M. Son, J. Shin, J. Park, J. Lee, S. Park, and H. Hwang, Nanotechnology 22, 472702 (2011)

[12]E. Cha, J. Park, J. Woo, D. Lee, A. Prakash, and H. Hwang, Appl. Phys. Lett. **108**, 153502 (2016)

[13]S. Li, X. Liu, S. K. Nandi, D. K. Venkatachalam, and R. G. Elliman, Appl. Phys. Lett. 106, 212902 (2015)

[14]E. Cha, J. Woo, D. Lee, S. Lee, J. Song, Y. Koo, J. Lee, C.G. Park, M.Y. Yang, K. Kamiya, K. Shiraishi, B. Magyari-Kope, Y. Nishi, and H. Hwang, in 2013 IEEE Int. Electron Devices Meet. IEEE, 2013, pp. 10.5.1

[15]A. A. Bolzan, C. Fong, and B. J. Kennedy, *J. Solid St. Chem.* **113**, 9 (1991)

[16]K. Sakata, I. Nishida, M. Matsushima, and T. Sakata, *J. Phys. Soc. Japan* **27,** 506 (1969)

[17]J. Park, T. Hadamek, A. B. Posadas, E. Cha, A. A. Demkov, and H. Hwang, Scientific Reports **7**, 4068 (2017)

[18]J.H. Lee, E.J. Cha, Y.T. Kim, B.K. Chae, J.J. Kim, S.Y. Lee, H.S. Hwang, C.G. Park, Micron **79**, 101 (2015)

[19]T. Joshi, T. R. Senty, P. Borisov, A. D. Bristow and D. Lederman, J. Phys. D: Appl. Phys. **48**, 335308 (2015)

[20]T. Joshi, P. Borisov, and D. Lederman, AIP Advances **6**, 125006 (2016)

[21]Grier, D., McCarthy, G., North Dakota State University, Fargo, North Dakota, USA. ICDD Grant-in-Aid (1991)

[22]M. Bj¨orck and G. Andersson, Journal of Applied Crystallography **40**, 1174 (2007)

[23]C. Lin, A. Posadas, T. Hadamek, and A. A. Demkov, PHYSICAL REVIEW B **92**, 035110 (2015)

[24]F. J. Wong, N. Hong, and S. Ramanathan, Phys. Rev. B **90**, 115135 (2014)

[25]I. H. Inoue, S. Yasuda, H. Akinaga, and H. Takagi, Phys. Rev. B 77, 035105 (2008)
[26]R. Meyer, L. Schloss, J. Brewer, R. Lambertson, W. Kinney, J. Sanchez, and D. Rinerson, Proc. 9th annual non-volatile Memory Tech. Symp. pp 54 (2008)
[27]Y. Wang, R. B.Comes, S. A. Wolf, and J. Lu, J. Electron Device Soc. 4, 11 (2016)
[28]W. A. Hubbard, T. Joshi, P. Borisov, D. Lederman, and B.C. Regan, Microsc. Microanal. 22 (S3), 2016
[29] J. Frenkel, Phys. Rev. 54, 647 (1938)
[30]A. Ongaro, A. Pillonnet, IEEE Proceeding 138, 127 (1991)
[31]S. Slesazeck, H. Mahne, H. Wylezich, A. Wachowiak, J. Radhakrishnan, A. Ascoli, R. Tetzlaff and T. Mikolajicka, RSC Adv. 5, 102318 (2015)
[32]G. A. Gibson, S. Musunuru, J. Zhang, K. Vandenberghe, J. Lee, C.-C. Hsieh, W. Jackson, Y. Jeon, D. Henze, Z. Li, and R. S. Williams, Appl. Phys. Lett. **108**, 023505 (2016)
[33]C. Funck, S. Menzel, N. Aslam, H. Zhang, A. Hardtdegen, R. Waser, and S. Hoffmann-Eifert, Adv. Electron. Mater. 2, 1600169 (2016)
[34]K. M. Kim, J. Zhang, C. Graves, J. J. Yang, B. J. Choi, C. S. Hwang, Z. Li, and R. S. Williams, Nano Letters 16, 6724 (2016)
[35]S.-E. Ahn, M.-J. Lee, Y. Park, B. S. Kang, C. B. Lee, K. H. Kim, S. Seo, D.-S. Suh, D.-C. Kim, J. Hur, W. Xianyu, G. Stefanovich, H. A. Yin, I.- K. Yoo, A.-H. Lee, J.-B. Park, I.-G. Baek, and B. H. Park, Adv. Mater. 20, 924 (2008)
[36] P. R. Shrestha, D. M. Nminibapiel, J. P. Campbell, J. T. Ryan, D. Veksler, H. Baumgart and K. P. Cheung, IEEE Trans. Electron. Dev. 65, 108 (2018)
[37]Chopra K L 1963 Proc. IEEE 51 941
[38]Geppert D V 1963 Proc. IEEE 51 223
[39]S. O. Pearson and H. St. G. Anson, Proc. Phys. Soc. of London 34, 204 (1921)
[40]A. A. Velichko, A. L. Pergament, G. B. Stefanovich and P. P. Boriskov, J. Sel. Top. Nano Electron. Comput. 2, 1 (2014)
[41]B. Ialevic and M. Shoga, Thin solid films, 75, 199 (1981)

List of Figures:

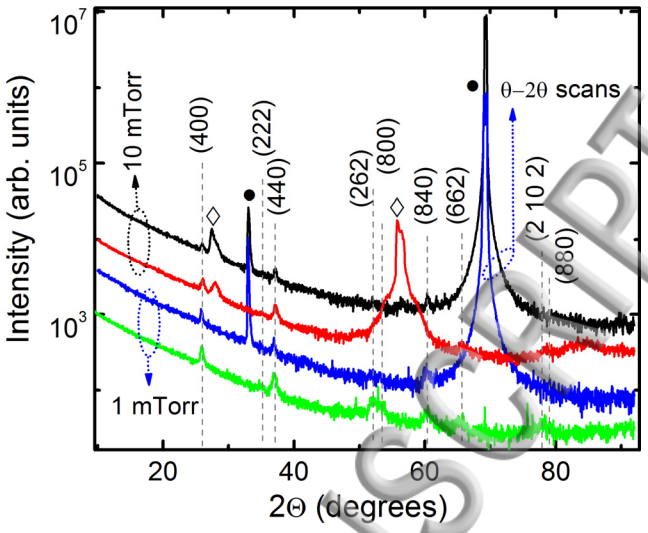

Figure 1: X-ray diffraction spectra. θ-2θ (black and blue curves) and grazing incidence x-ray diffraction (GIXRD) (red and green curves) patterns of NbO_2 films grown in 1 (green and blue curves) and 10 mTorr (red and black curves) total pressure. Sharp peaks denoted by '●' and '◊' are from (100) Si and (010) SiO_2, respectively. The dotted lines indicate the bulk peak positions from PDF# 000-43-1043. The grazing incidence angle was $\alpha = 3^{\circ}$.

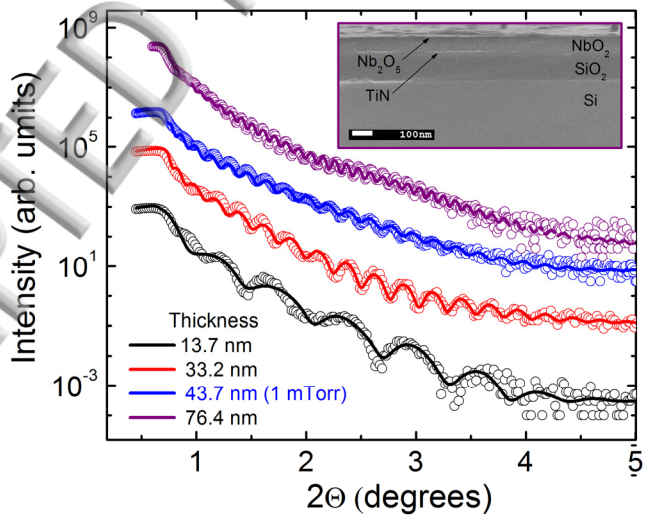

Figure 2: X-ray reflectivity (XRR) data (open circles) for NbO_2 films with the corresponding fits (solid lines). All films were grown in 10 mTorr total pressure, except the 43.7 nm film grown in 1mTorr total pressure. Inset figure shows the cross-sectional SEM image of the 76.4 nm thin film.

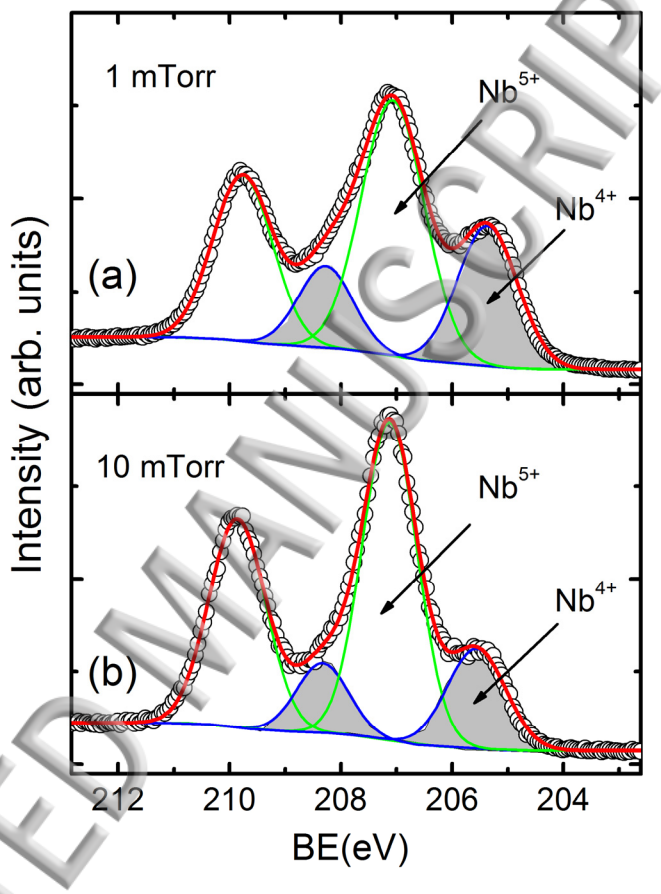

Figure 3: X-ray photoelectron spectroscopy (XPS) data for Nb $3d_{5/2}$ and $Nb_{3/2}$ spectra of films grown in 1 mTorr (a) and 10 mTorr (b) growth pressures with deconvoluted peak fits. The shaded areas are the contribution from the Nb^{4+} valency state. The molar content of NbO_2/Nb_2O_5, estimated using areas covered by $3d_{5/2}$ level speaks, was found as 34.2%/65.8% and 25.1%/74.9% for the film grown in 1 and 10 mTorr, respectively.

This manuscript was accepted by J. Appl. Phys. Click here to see the version of record.

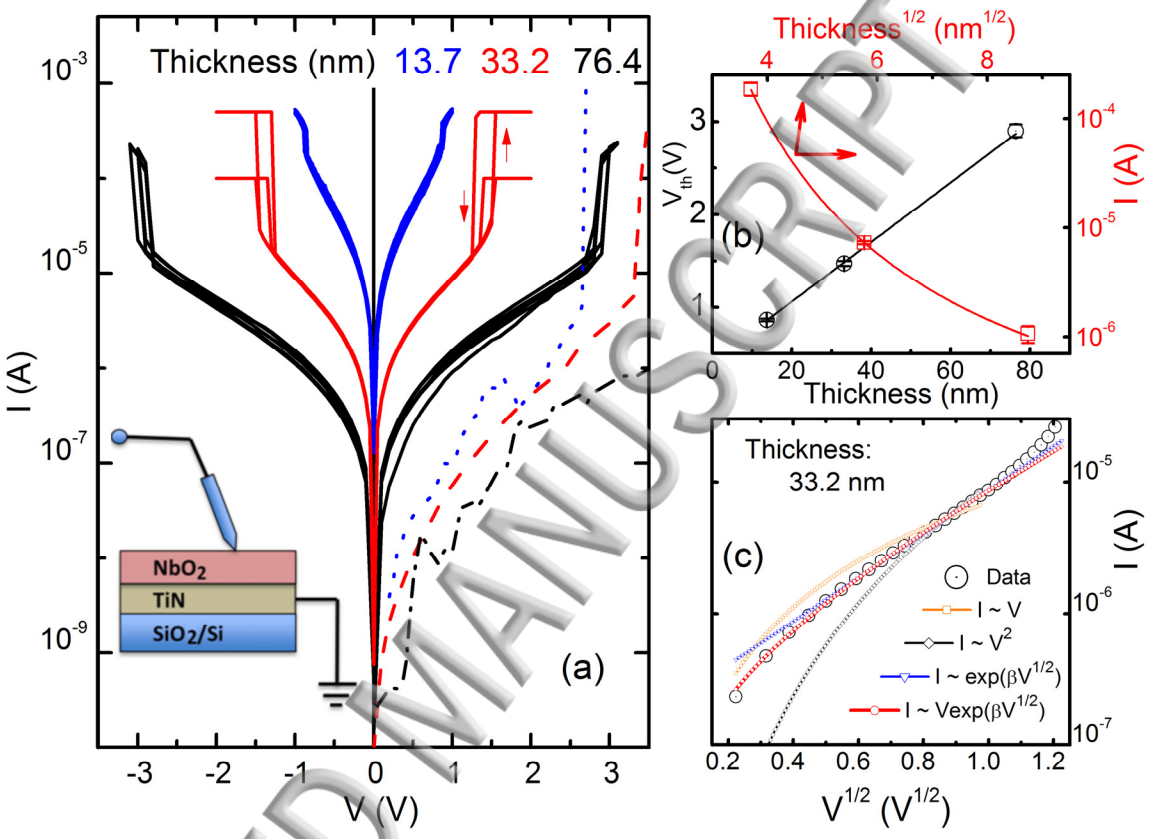

Figure 4: (a) *I-V* curves measured using probe station tungsten tip at RT in the air on films of different thicknesses. Inset: schematics of sample structure and measurement setup. Arrows indicate the direction of voltage sweep. The forming sweeps are represented by dotted (13.7 nm), dashed (33.2 nm) and dashed-dotted (76.4 nm) type curves. (b) The threshold voltage (V_{th}) plotted against film thickness and current measured at V = 0.9 V plotted against (thickness)$^{1/2}$. Solid lines are fits. (c) Experimental ln(*I*) *vs.* $V^{1/2}$ graphed for 33.2 nm NbO_2 film below 1 V with fits to the following conduction models: Ohmic ($I \sim V$), space-charge-limited ($I \sim V^2$), Schottky [$I \sim \exp(\beta V^{\frac{1}{2}})$] and Poole-Frankel conduction [$I \sim V\exp(\beta V^{1/2})$].

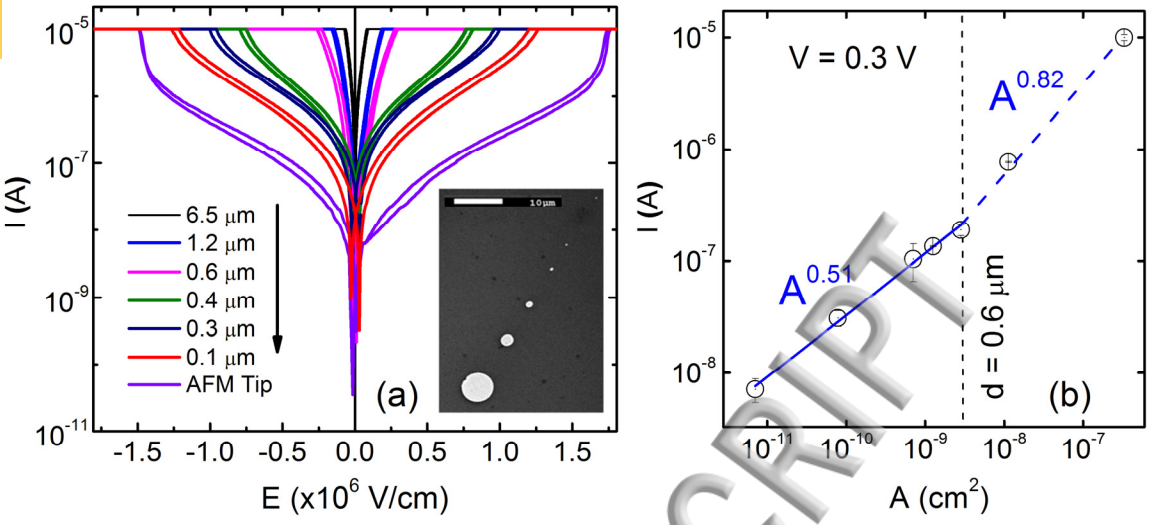

Figure 5: Contact size dependent *I-V*. (a) *I-V* curves measured using conducting probe AFM at RT in the air for the film grown in 10 mTorr pressure using different electrode sizes (inset: SEM image of the top electrodes). (b) Current measured at 0.3 V vs. top contact area A. Solid lines represent linear fits on the log-log scale to the current $I \propto A^n$, where A is the area of the top electrode, and n is the exponent.

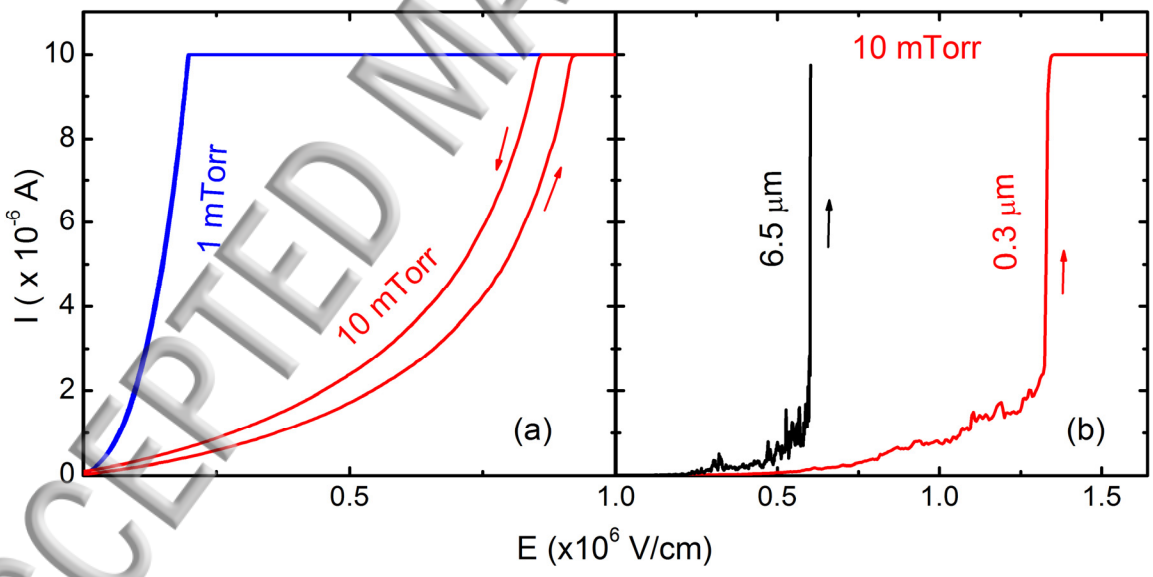

Figure 6: (a) *I-V* curves obtained from the films grown in 1 mTorr and 10 mTorr films using 0.3 μm contacts. (b) Two of the forming pulses for the film grown in 10 mTorr with contacts 6.5 and 0.3 μm. Arrows indicate the direction of voltage sweep.

This manuscript was accepted by J. Appl. Phys. Click here to see the version of record.

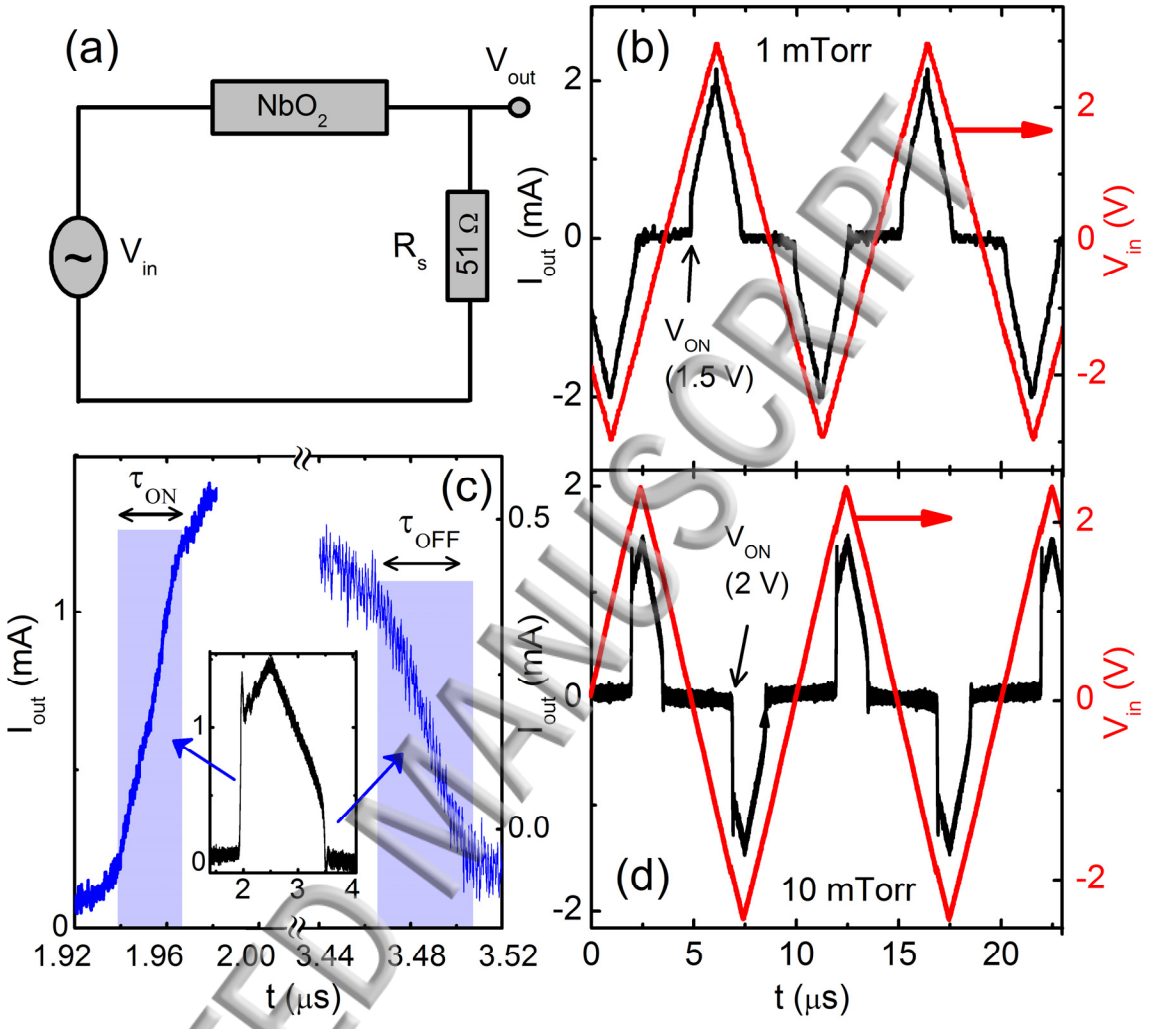

Figure 7: Pulsed *I-V* measurement. (a) Circuit diagram. (b), (d) Pulsed input (right scale) and output current characteristics obtained from films grown in 1 and 10 mTorr films, respectively. (c) A zoomed part of (d) showing current switching times: τ_{ON} = 25 ns and τ_{OFF} = 40 ns.

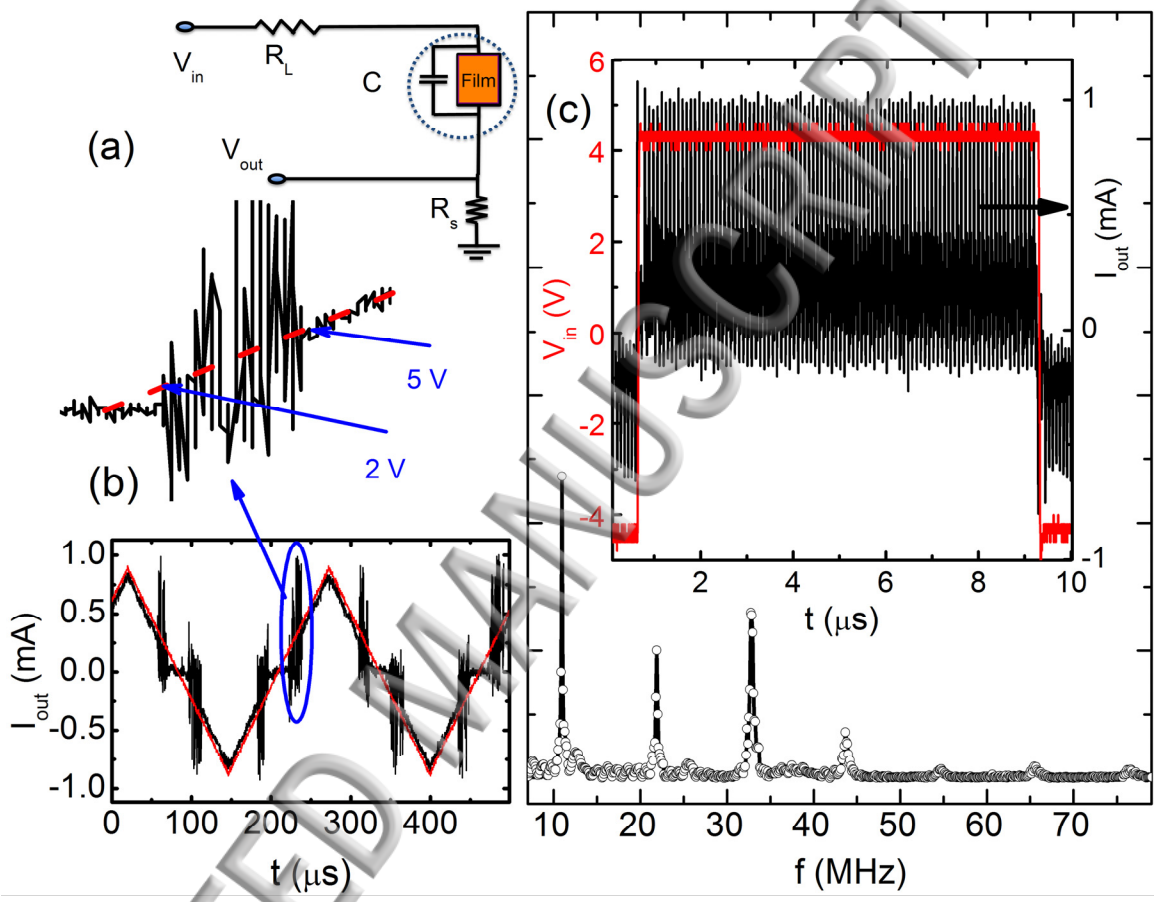

Figure 8: Self-sustained current oscillations obtained from the film grown in 1 mTorr pressure. (a) Schematic diagram for a current oscillator. (b) Current oscillations produced by a triangular pulse field. The zoomed figure showed the range of input voltage contributing for oscillation was 2 V to 5 V. (c) Self-sustained current oscillations measured from the film grown in 1 mTorr growth pressure using a rectangular pulse field with Fast Fourier Transform (FFT) showing fundamental frequency at 11 MHz.

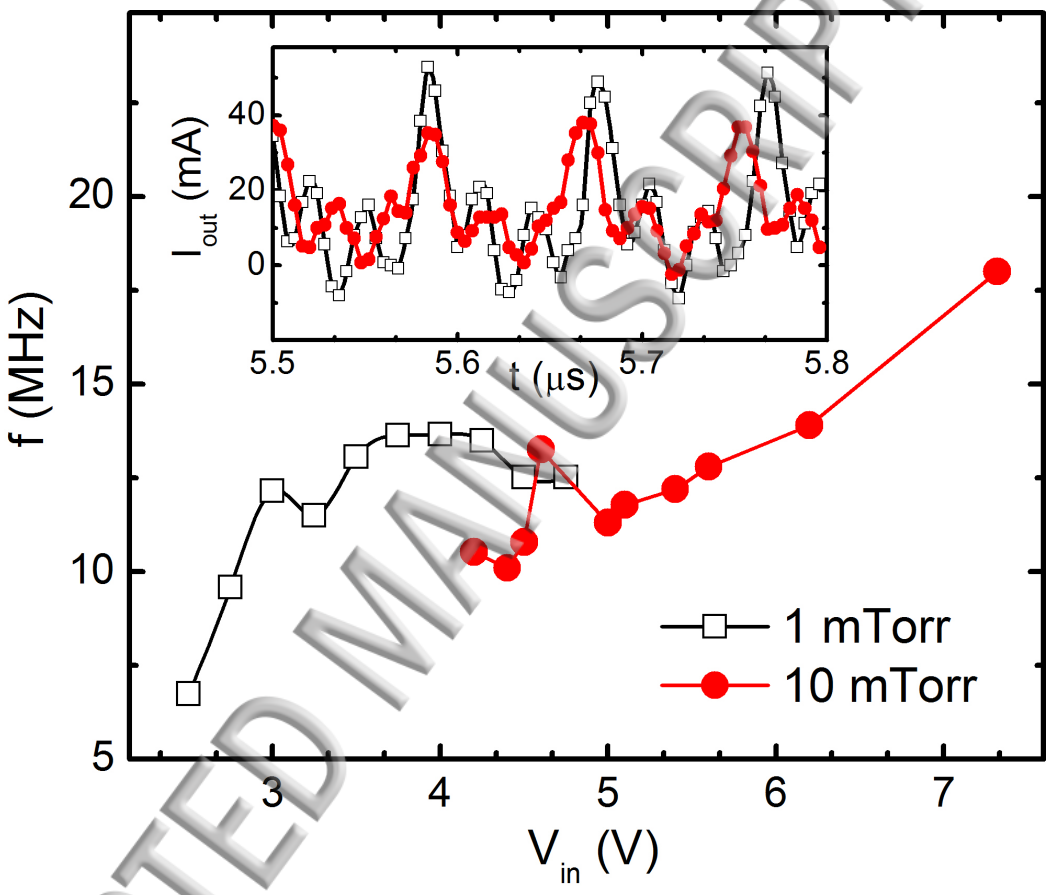

Figure 9: Input *V* versus *f* of films grown in 1 and 10 mTorr pressures. Inset figure shows zoomed view of current oscillations with similar frequency about 11 MHz measured on both films grown in 1 and 10 mTorr growth pressure.

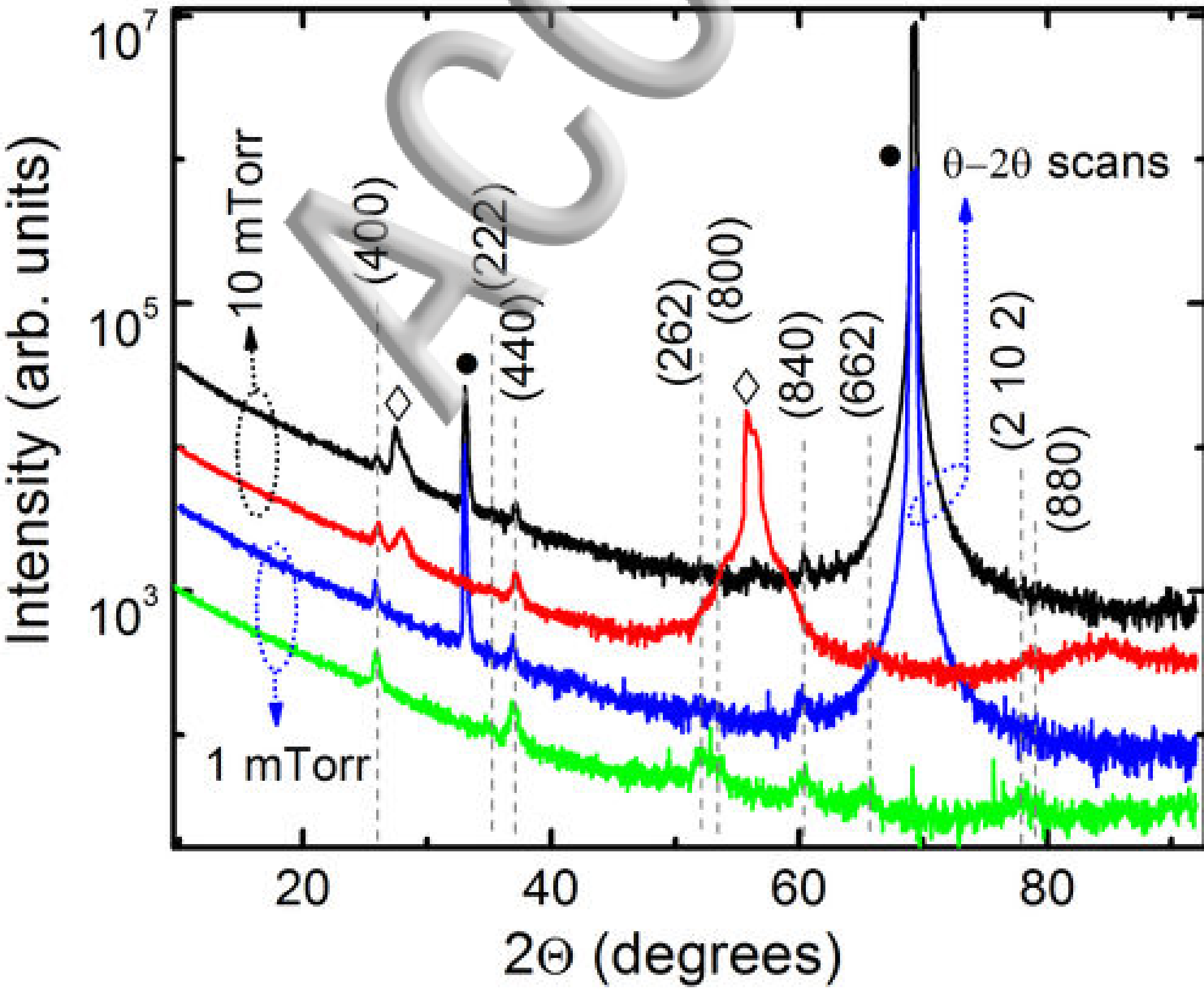
Intensity (arb. units)
10^7
10^5
10^3
10 mTorr
1 mTorr
(400)
(222)
(440)
(262)
(800)
(840)
(662)
(2 10 2)
(880)
θ–2θ scans
20
40
60
80
2Θ (degrees)

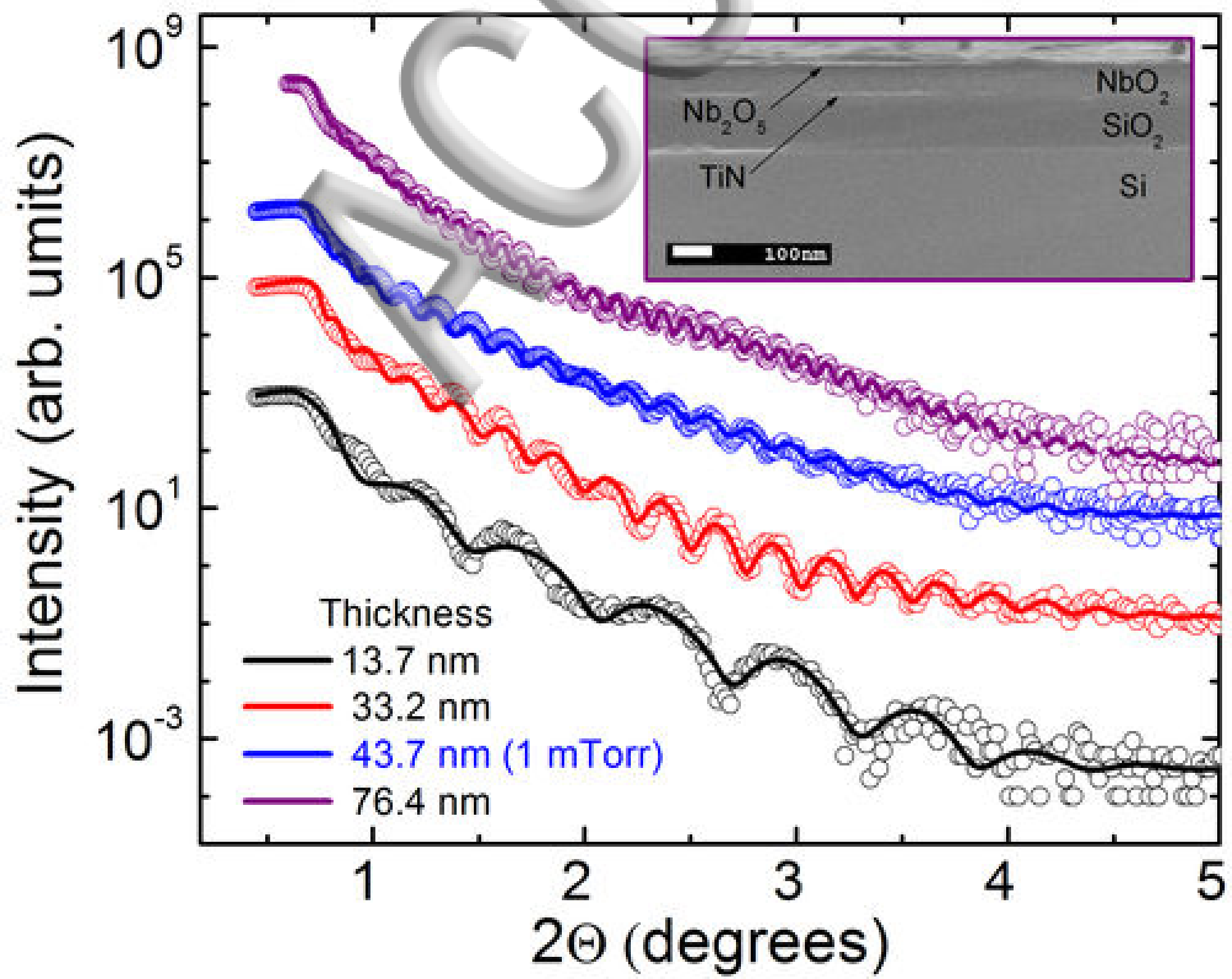
Intensity (arb. umits)
10^9
10^5
10^1
10^-3
1
2
3
4
5
2Θ (degrees)
Thickness
13.7 nm
33.2 nm
43.7 nm (1 mTorr)
76.4 nm
Nb2O5
TiN
NbO2
SiO2
Si
100nm

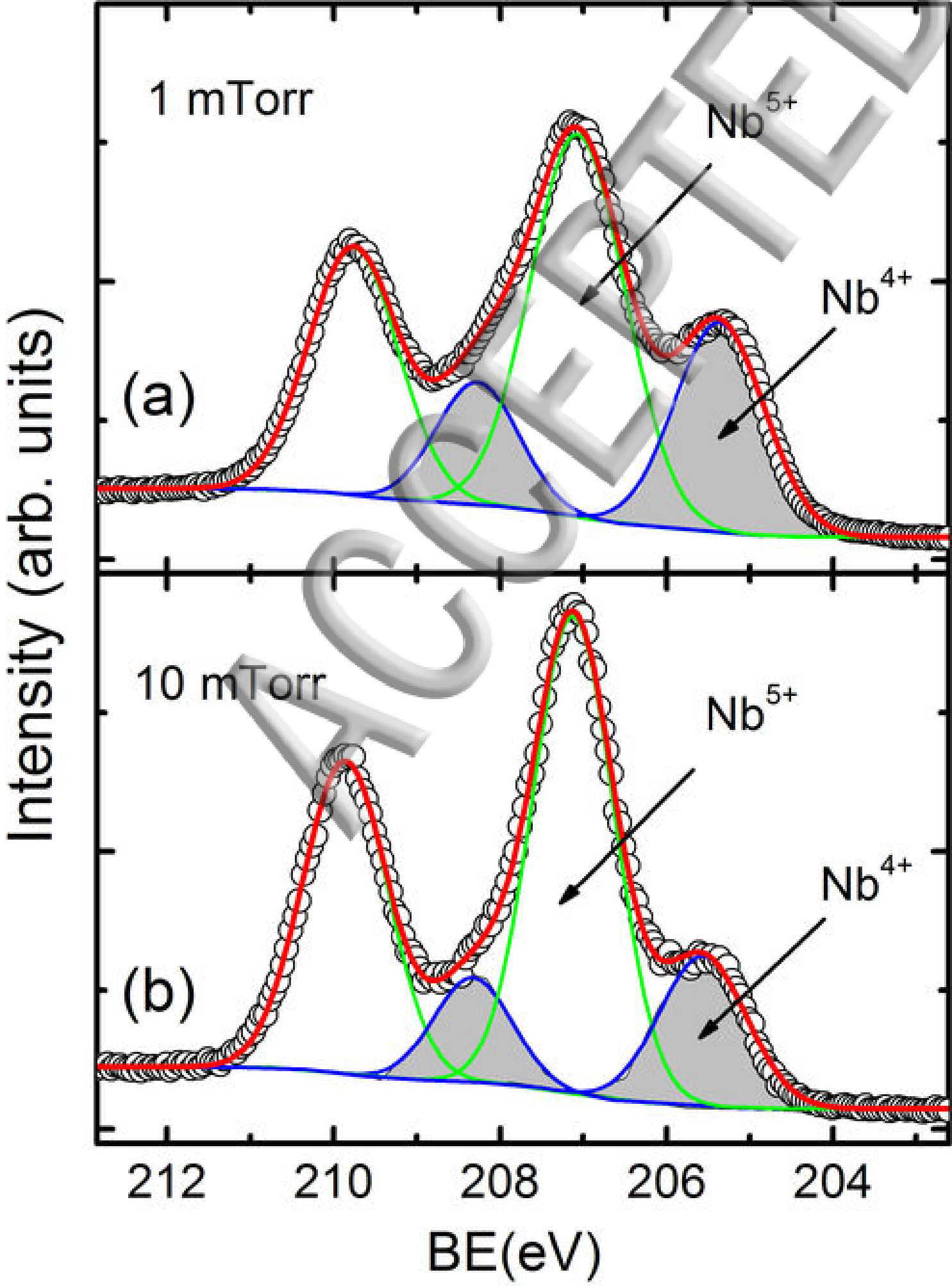
1 mTorr
Nb5+
Nb4+
(a)
10 mTorr
Nb5+
Nb4+
(b)
Intensity (arb. units)
212
210
208
206
204
BE(eV)

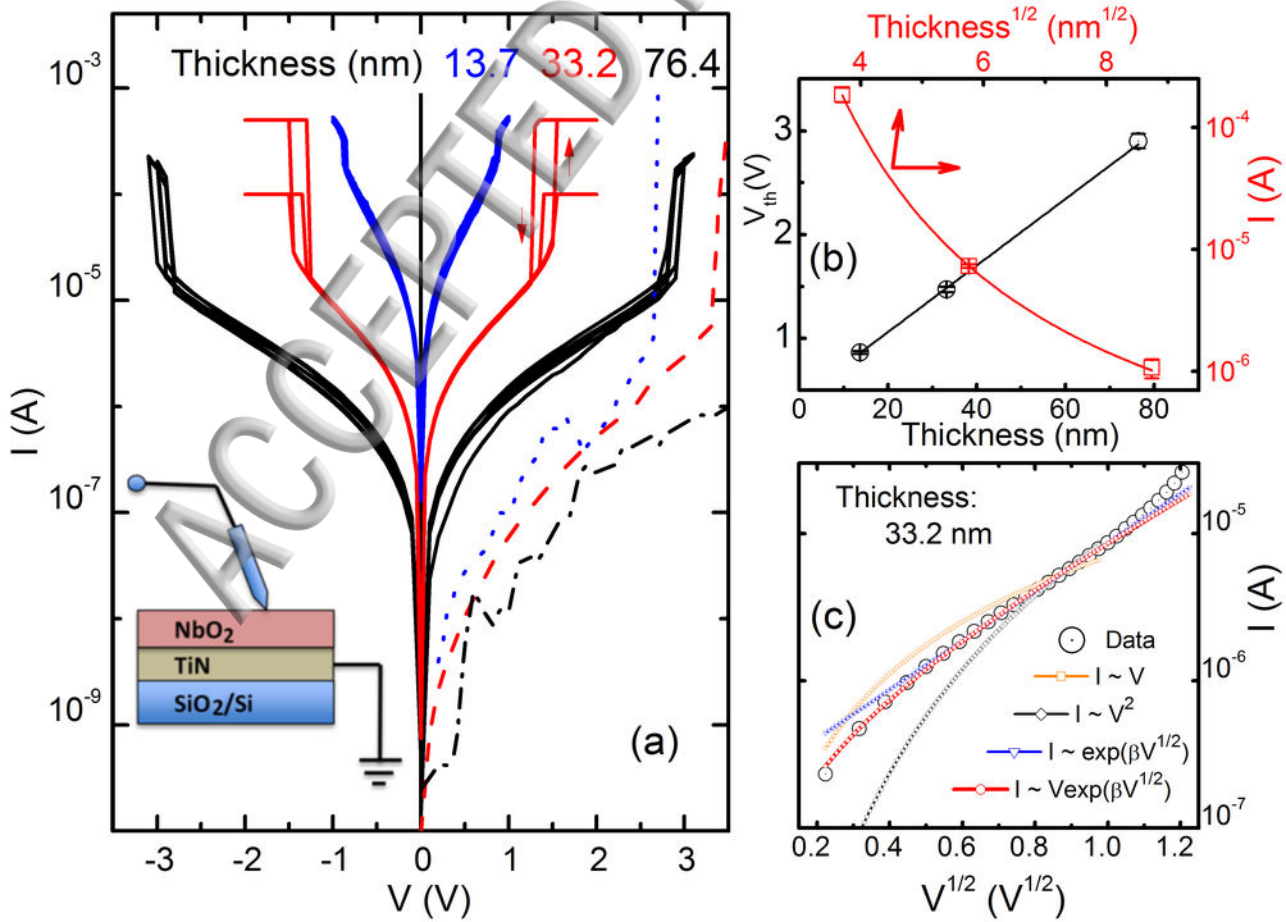
Thickness (nm) 13.7 33.2 76.4
I (A)
V (V)
(a)
NbO2
TiN
SiO2/Si
Thickness1/2 (nm1/2)
Vth (V)
(b)
Thickness (nm)
Thickness:
33.2 nm
(c)
Data
I ~ V
I ~ V2
I ~ exp(βV1/2)
I ~ Vexp(βV1/2)
V1/2 (V1/2)

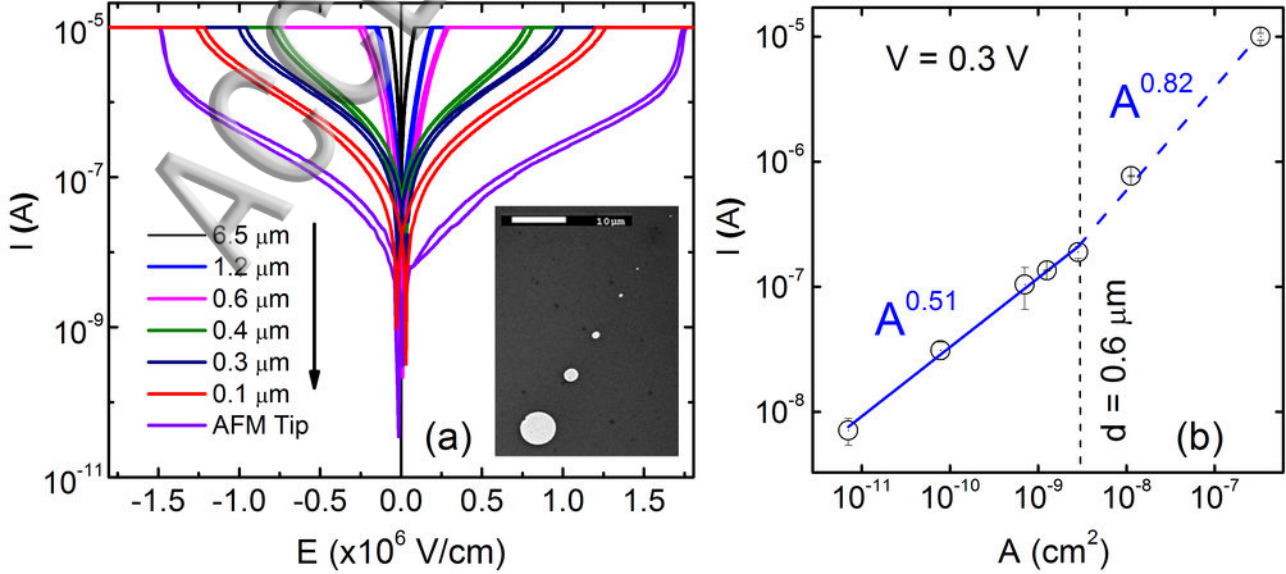
I (A)
E (x10^6 V/cm)
6.5 μm
1.2 μm
0.6 μm
0.4 μm
0.3 μm
0.1 μm
AFM Tip
(a)
10μm
V = 0.3 V
A^0.51
A^0.82
d = 0.6 μm
(b)
A (cm^2)

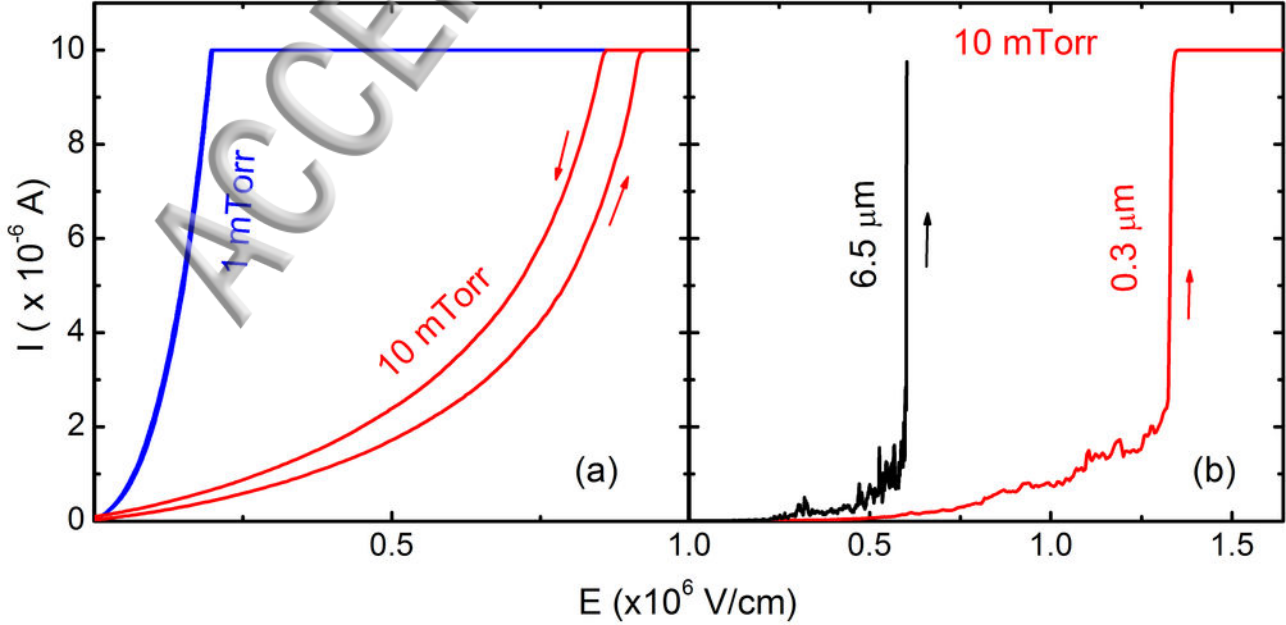
I (x 10^-6 A)
E (x10^6 V/cm)
1 mTorr
10 mTorr
(a)
10 mTorr
6.5 μm
0.3 μm
(b)

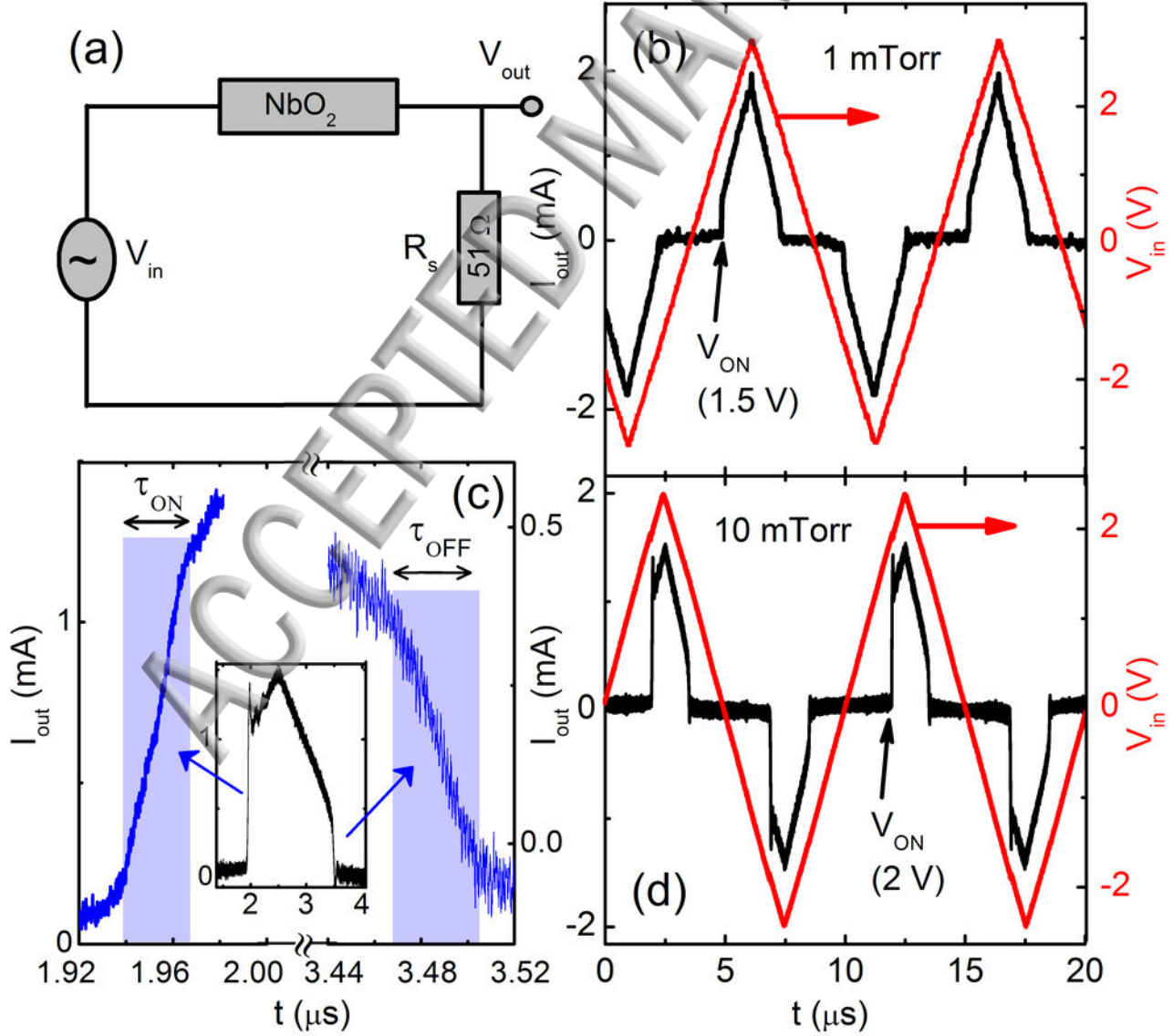
(a)
V_{out}
NbO_2
V_{in}
R_s
51 Ω
(b)
1 mTorr
V_{ON}
(1.5 V)
I_{out} (mA)
V_{in} (V)
(c)
τ_{ON}
τ_{OFF}
(d)
10 mTorr
V_{ON}
(2 V)
t (μs)

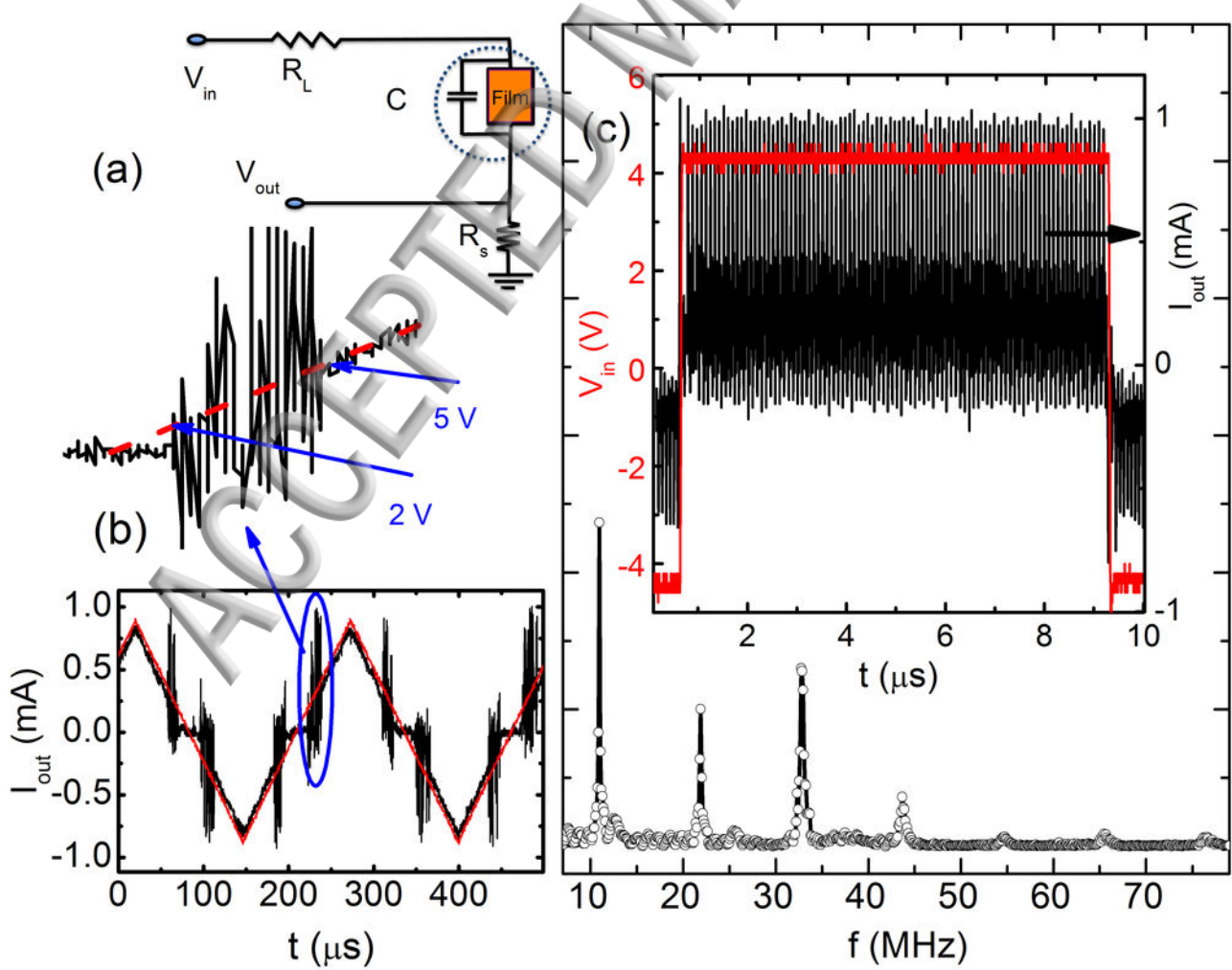

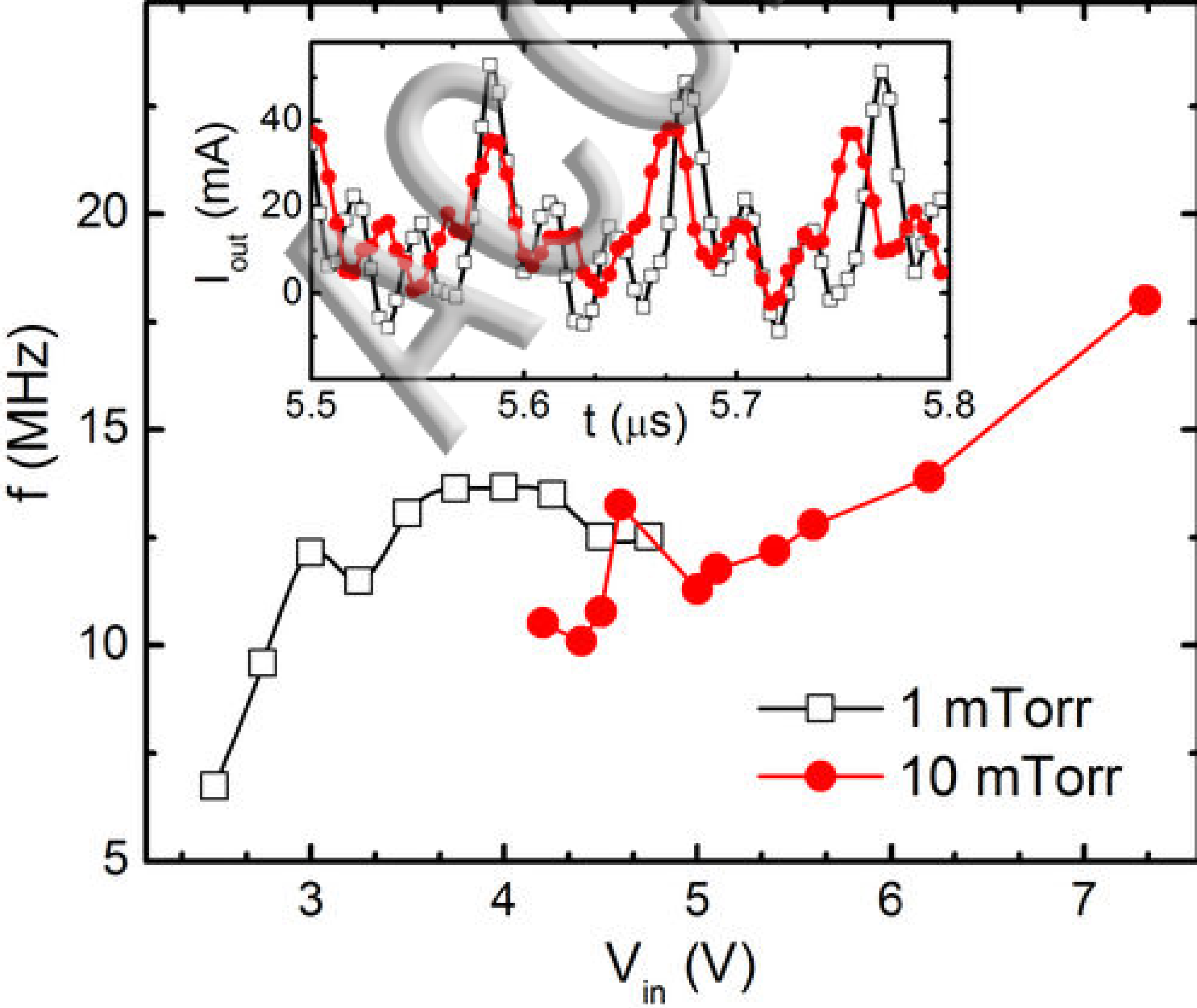
f (MHz)
20
15
10
5
3
4
5
6
7
V_{in} (V)
1 mTorr
10 mTorr
I_{out} (mA)
40
20
0
5.5
5.6
t (μs)
5.7
5.8